J. Fluid Mech. (1990), *vol.* 210, *pp.* 303–328
Printed in Great Britain

Marangoni effects of trace impurities on the motion of long gas bubbles in capillaries

By J. RATULOWSKI AND H.-C. CHANG
Department of Chemical Engineering, University of Notre Dame, Notre Dame, IN 46556, USA

(Received 16 November 1988 and in revised form 22 June 1989)

When a viscous liquid is displaced by a long air bubble in a capillary, it leaves behind a wetting liquid film. A lubrication analysis by Bretherton (1961), which assumes a mobile surface, underpredicts the film thickness at low bubble speeds. In this investigation, the Marangoni effect of small amounts of impurities is shown to be capable of explaining this discrepancy. We carry out an asymptotic analysis for different convective, diffusive and kinetic timescales and show that, if transport in the film is mass-transfer limited such that a bulk concentration gradient exists in the film, the film thickness increases by a maximum factor of $4^{\frac{2}{3}}$ over Bretherton's mobile result at low bubble speeds. Moreover, at large bubble speeds, Bretherton's mobile prediction is approached for all ranges of timescales. For intermediate bubble speeds, the film thickness varies with respect to the bubble speed with an exponent smaller than $\frac{2}{3}$ of the mobile theory. These results are favourably compared to literature data on film thickness.

1. Introduction

The displacement of a viscous wetting fluid by an inviscid fluid in circular capillaries and between closely spaced flat plates has been studied extensively both theoretically and experimentally. Fairbrother & Stubbs (1935) noted that a wetting film is deposited on the wall of a capillary as a wetting viscous fluid is displaced by a gas bubble. Dimensional analysis indicates that the wetting film thickness at low bubble speeds is only a function of capillary number $Ca = \mu U/\gamma$ where μ is the wetting phase viscosity, U the bubble velocity, and γ the surface tension. The capillary number is the ratio of viscous to capillary effects. The experimental results of Fairbrother & Stubbs for air displacing water in circular tubes indicated that, in the range of Ca of 7.5×10^{-5} to 0.014, the wetting film thickness was proportional to $Ca^{\frac{1}{2}}$. Subsequent experimental work of Taylor (1961) confirmed this finding and extended it to higher Ca. For very large Ca, Taylor found that the wetting film thickness no longer followed the $\frac{1}{2}$ power law but asymptotically approached a constant value near 0.55 of the capillary radius. Wetting film thickness in an air–water system measured experimentally with a technique based on electrical conductivity by Marchessault & Mason (1960) for capillary numbers from 10^{-5} to approximately 10^{-4} were somewhat larger than those predicted by the Fairbrother–Stubbs correlation.

Bretherton (1961) first used elements of asymptotic matching to predict wetting film thickness and the pressure drop across a long bubble moving in a circular capillary. The approach of Bretherton was similar to that used by Landau & Levich (1942) for the coating of a flat plate by the withdrawal of the plate from a stagnant pool of liquid. A set of equations valid in the thin film region obtained through

lubrication arguments was matched to a region of static curvature at the front of the bubble. In the limit of low capillary number, the theory predicted that the wetting film thickness was proportional to $Ca^{\frac{2}{3}}$. Bretherton measured film thickness for the displacement of two polar organic liquids, aniline and benzene, over a large range of capillary numbers, 10^{-6} to 10^{-2}, by measuring the decrease in volume of the liquid slug preceding the bubble front. The change in volume of the slug could be directly related to the film thickness by assuming that a stagnant film was deposited. Good agreement between theory and experiment was found above Ca of 10^{-3}. However, below 10^{-3} the measured film thickness was significantly larger than the theoretical predictions (see figure 8). Because an asymptotic theory for low Ca should become better as Ca decreases, this surprising experimental result placed the validity of the model in doubt. Bretherton offered several explanations for the discrepancy between theory and experiment. These include surface roughness, instability of the meniscus, intermolecular forces, and adsorbed impurities.

Park & Homsy (1984) used formal perturbation techniques to confirm and extend the Bretherton results for the displacement of a viscous fluid between flat plates. Goldsmith & Mason (1963) first considered both theoretically and experimentally drops with non-zero dispersed phase viscosity. However, as we shall demonstrate subsequently, they incorrectly proposed that the effect of surfactants could be modelled simply with a finite shear at the bubble interface. Teletzke (1983) and Schwartz, Princen & Kiss (1986) formally modified the Bretherton approach to include the effects of a finite dispersed phase viscosity and intermolecular forces (London dispersion and electrostatic repulsion). Neither effect could explain the magnitude of the deviation between experiment and theory at low Ca. The viscosity of gas is certainly much smaller (by a factor of 50) than that of the liquid and is not a function of Ca. Consequently, the assumption of an inviscid bubble is valid and the inclusion of a finite dispersed phase viscosity cannot explain why the deviation occurs only at low Ca. In the case of intermolecular forces, calculations carried out by Teletzke (1983) for reasonable estimates of the London dispersion forces indicate that the film thickness in the Bretherton experiments is at least an order of magnitude larger than the thickness at which intermolecular forces should become significant. Recently, Chen (1986) has experimentally measured the film thickness of long and short bubbles in very small circular capillaries with a technique similar to Taylor's measurements. Again, a significant deviation at low Ca from the Bretherton theory was observed. Chen attributed this effect to surface roughness and supported his assumption with photographs of the capillary walls. In Chen's experiments, wall roughness can indeed explain the low Ca behaviour of the film thickness. However, this is not true of the original Bretherton experiments. Bretherton observed that different wetting liquids had different low Ca behaviour (see figure 8). If surface roughness caused the film thickness to approach a constant value as Ca decreased, the asymptotic value should be independent of the wetting liquid used in the experiments. Schwartz *et al.* (1986) have repeated Bretherton's experiments for long and short bubbles. Their measured film thickness for long bubbles is more closely modelled by the Fairbrother–Stubbs correlation than the Bretherton theory. The measured film thickness is always larger than the Bretherton prediction and the deviation is more pronounced at lower Ca. Schwartz *et al.* reject Chen's argument that surface roughness is the cause of their observed film thickness. Because the capillaries in their experiments were larger than those in Chen's experiments, the measured film thicknesses were larger. Consequently, the size of the surface irregularities required to explain the deviation of the measured film thickness from

the Bretherton result must also be proportionally larger. Such large surface irregularities were not found. Schwartz *et al.*'s arguments are supported by the data presented in figure 8. Only Chen's data exhibit the unusual constant tail at relatively large Ca.

Both Bretherton and Teletzke have suggested that the cause of the discrepancy between theory and experiment is a small amount of adsorbed surface-active contaminants on the interface. Bretherton terms this effect surface hardening and likens it to the retarding effect of adsorbed surfactants on the motion of spherical drops and bubbles in an infinite viscous medium. This problem has been studied by several investigators (Levich 1962; Davis & Acrivos 1966; Sadhal & Johnson 1983). Here, the surfactant is swept to the back of an advancing bubble and accumulates near the rear. In regions of low surfactant concentration the interface is mobile. That is, the stress-free condition is approximately obeyed. However, in regions of high surfactant concentration, the interface becomes nearly rigid and is more closely described by a no-slip condition. Bretherton conjectured that the maximum retarding effect of the surfactants would be to cause the entire interface to behave rigidly. Integration of a new set of lubrication equations in which the no-slip condition is imposed everywhere in the transition region resulted in an increase in film thickness by a constant factor of $2^{\frac{2}{3}}$. This increase in theoretical film thickness was not sufficient to explain the low Ca benzene film thickness and did not provide a reason for the apparent Ca dependence of the error in the asymptotic theory. In fact, a long moving rigid bubble with constant surface tension cannot lay down a flat film. A flat and rigid interface translating at a constant velocity induces a linear Couette flow field within the film. This implies that a finite net tangential shear exists on the interface which violates the jump stress balance on a free surface. This can only be balanced by a gradient in the surface tension which is not included in the rigid bubble model of Bretherton (1961) and Goldsmith & Mason (1963). If the tangential stress boundary condition is omitted, the interface cannot be viewed as a free surface and the interface profile should then be specified and not computed. In fact, in the studies of spherical drops and bubbles in an infinite fluid (Levich 1962; Davis & Acrivos 1966; Sadhal & Johnson 1983), the free surface is specified to be a sphere and the net drag force is then computed. In the present problem, the film profile is the solution sought and the tangential stress balance must be satisfied. Recently, Herbolzheimer (1987) reported a simple limiting model to overcome this shortcoming of the constant-shear rigid bubble model. In his model, the rigid bubble interface is completely stationary in the laboratory frame such that there is no flow (or shear) at all in the flat film. He showed that the film thickness is increased by a maximum factor of $4^{\frac{2}{3}}$. This indeed bounds most data although, since the correction is independent of Ca, this limiting model is incapable of explaining the smaller exponent of the film thickness dependence on Ca, such as the 0.5 of Fairbrother & Stubbs' correlation instead of $\frac{2}{3}$ of Bretherton's theory and it does not explain why Bretherton's mobile result is approached at high Ca in all experiments. Herbolzheimer's model is our stationary-surface model in figure 3 which we derived independently and reported at the same meeting (Chang & Ratulowski 1987).

If the effect of surface-active contaminant is to be correctly assessed, the variation of surface tension along the interface must be modelled. Surface tension is a function of surfactant concentration at the interface, owing to the Marangoni effect (Levich 1962). Consequently, when a bubble moves and gradients in surfactant result from transport of surfactant along the interface, there exists a gradient in surface tension

which balances the tangential shear at the interface. The ability of the interface to support a tangential stress in the surfactant system is the surface hardening phenomenon described by Bretherton. However, the degree of surface hardening is a function not only of the relation between surface tension and surfactant concentration but also of the transport of surfactants both in the bulk phase and on the interface. Teletzke (1983) and Schwartz *et al.* (1986) have modified the original Bretherton lubrication equation by including the surface tension gradient via the tangential stress balance at the interface. However, no attempt was made to model this term by addressing the surfactant transport problem. In both cases, a constant value was assigned to the gradient. Schwartz *et al.* argued that the film thickness measured by the Bretherton method would actually be smaller than in a pure system because of liquid flow in the thin film induced by the non-zero surface traction. The opposite was observed experimentally. Therefore, the surfactant effect was discounted by Schwartz *et al.* as the cause of the error in Bretherton's theory. In their model, surface tension is assumed to be higher at the nose of the bubble and lower in the flat-film region. While this is consistent with the model for bubbles moving in an infinite viscous fluid (Levich 1962; Davis & Acrivos 1966), we shall show that the opposite is true for the present problem of bubbles in capillaries under certain limiting conditions. Hirasaki & Lawson (1985) have attempted to include the interfacial transport of surfactant in a solution of the lubrication equations in the uniform film region. The bulk phase surfactant concentration was assumed to be constant, thus removing the need to solve the bulk phase transport problem. In their analysis, the film thickness was assumed to be a constant and was not obtained through a matching to the front cap region. Instead, it was left as a parameter to be fitted empirically. Ginley & Radke (1989) have improved Hirasaki & Lawson's model by including surface transport of the surfactants while still neglecting all concentration gradients in the bulk. With their formulation, the film profile can be determined. They find by perturbing about infinite adsorption rate that there is a decrease in the film thickness due to surface tension gradient. Ginley & Radke's model is our bulk equilibrium model in figure 3. We shall show that an increase in film thickness occurs if surfactant transport in the bulk is mass-transfer limited such that a concentration gradient exists.

In this paper, we carry out an asymptotic analysis of the transport of surfactants in both the bulk liquid and the interface. We show that, to explain the increased film thickness due to the Marangoni effect of trace impurities, a concentration gradient must exist in the bulk liquid to overcome the negative effects of surface convection. Through the adsorption kinetics, this bulk gradient causes the surface concentration to decrease downstream from the bubble cap to the thin film. The surface tension in the film is then larger than its value at the cap and a surface traction in the direction of the film is created (see figure 1). This, in turn, induces more liquid to flow into the film than the mobile case, thus producing a thicker film. At large Ca, however, the horizontal velocity becomes so large that the surface concentration gradient does not cause enough traction to yield a noticeable alteration of the flow field. Hence, the observed discrepancy of the film thickness at low Ca is because the Marangoni effect is most significant in that limit. In the next section, we present the full governing equations for momentum and surfactant transport for this problem. A perturbation analysis of the equation of motion is presented in §3. In §4, a lubrication analysis of the bulk and interface surfactant transport equations is carried out for various convective, diffusive and kinetic timescales. It is shown that, if bulk concentration gradient exists and adsorption kinetics is fast, the traction is negative throughout

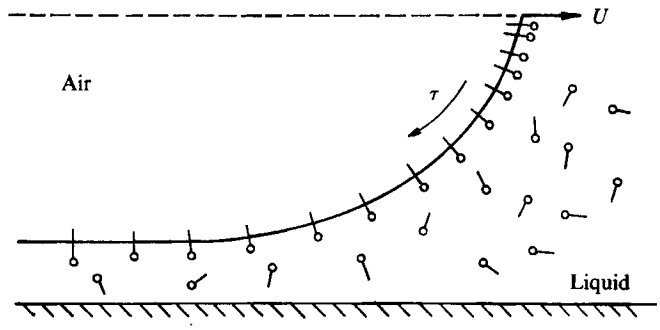

FIGURE 1. Schematic of an air bubble travelling in the positive x-direction in a circular capillary. Depicted is the negative traction caused by a decreasing surface concentration into the film in our convective-equilibrium model.

the film and the maximum correction at low Ca is $4\frac{2}{3}$. In §5, two of the models with bulk gradient are solved numerically to obtain the film thickness and the pressure drop across the frong cap. These are favourably compared to experimental data.

2. Governing equations

Consider a semi-infinite bubble moving at a constant velocity U in a circular capillary of radius R as shown in figure 1. We employ a coordinate system moving at the same speed U relative to the stationary laboratory frame in the axial direction x. The bubble interface is stationary in this coordinate with a spherical cap at the bubble front and a flat film region at $x \to -\infty$. We shall not consider the back half of the bubble since the film thickness can be obtained from just the front half (Bretherton 1961; Lu & Chang 1988; Ratulowski & Chang 1989). The upstream far field ($x \to \infty$) bulk concentration of the surfactant is C_0. Since the surface tension varies along the interface S, we choose the reference surface tension γ_0 to be the value at the bubble tip. Using R, U, C_0, RC_0 and γ_0/R to scale length, velocity, bulk concentration, interfacial concentration and pressure, the dimensionless momentum and mass transport equations become

$$Ca\nabla^2 \boldsymbol{u} = \nabla p, \tag{2.1}$$

$$\nabla \cdot \boldsymbol{u} = 0, \tag{2.2}$$

$$\nabla \cdot (C\boldsymbol{u}) = \frac{1}{Pe}\nabla^2 C, \tag{2.3}$$

$$\nabla_\sigma \cdot (\Gamma \boldsymbol{u}^\sigma) = -\frac{1}{Pe}\boldsymbol{n} \cdot \nabla C \quad \text{on} \quad S, \tag{2.4}$$

where inertial, buoyancy and surface diffusion terms have been neglected. (In typical experiments with air and water in capillaries of approximately 1 mm diameter, the Reynolds number is less than 1.0×10^{-3} and the Bond number $\Delta\rho R^2/\gamma_0$ is approximately 5.0×10^{-4}.) The bulk and surface concentrations are denoted by C and Γ, respectively. The operator ∇_σ is the surface gradient on the interface S. The velocity field $\boldsymbol{u}^\sigma$ is the interfacial velocity and $\boldsymbol{n}$ is the unit normal vector of the interface S. The dimensionless parameters are the capillary number $Ca = \mu U/\gamma_0$ and Péclet number $Pe = UR/D$ where D is the bulk diffusivity.

The radial boundary conditions for the momentum transport equations are the no-slip condition on the capillary wall W

$$\boldsymbol{u} = -\boldsymbol{e}_x \quad \text{on} \quad W, \tag{2.5}$$

where $\boldsymbol{e}_x$ is the unit vector in the axial direction and the tangential and normal stress balances on S,

$$\boldsymbol{n}\cdot\boldsymbol{P} = 0 \quad \text{on} \quad S, \tag{2.6}$$

$$\boldsymbol{t}\cdot\boldsymbol{P} = 0 \quad \text{on} \quad S. \tag{2.7}$$

The vector $\boldsymbol{P}$ is

$$\boldsymbol{P} = \nabla_s\gamma + \kappa\gamma\boldsymbol{n} + p\boldsymbol{n} - Ca\boldsymbol{\tau}\cdot\boldsymbol{n}, \tag{2.8}$$

where γ is the dimensionless surface tension scaled with respect to γ_0, κ is the dimensionless surface curvature scaled by $1/R$ and $\boldsymbol{\tau}$ is the dimensionless stress tensor. In (2.6) and (2.7), the gas pressure is chosen to be zero and the gas phase is inviscid. The remaining interfacial condition is the kinematic condition which requires that

$$\boldsymbol{u}\cdot\boldsymbol{n} = 0 \quad \text{on} \quad S. \tag{2.9}$$

The momentum boundary conditions in the axial x-direction are that a Poiseuille profile exists at $x = +\infty$ and a flat profile, corresponding to a stationary film in laboratory coordinates, exists in the flat-film region $x = -\infty$,

$$\boldsymbol{u} \to -\boldsymbol{e}_x \quad \text{as} \quad x \to -\infty. \tag{2.10}$$

This limiting velocity boundary condition must be complemented by compatible limiting conditions for the interface and bulk surfactant concentrations since a flat velocity profile can only exist in a flat film if surface tension gradient, which is caused by surfactant concentration gradient, is absent. In a stationary film, both the interface and bulk surfactants are not convected and the only resistance arises from the rate of adsorption/desorption onto the interface. (As we shall show in §4, radial diffusion is extremely rapid in the thin film and is hence not a rate-limiting step.) This then requires the flat film region to be sufficiently long such that the surfactants have sufficient time to adsorb and equilibrate as they are swept into the flat-film region. We note that Schwartz *et al.* (1986) have discovered experimentally that at $Ca = 3.0 \times 10^{-5}$ short bubbles with bubble lengths shorter than 20 capillary radii show behaviour approaching the Bretherton theory for mobile interfaces while the positive correction scrutinized here only exists for long bubbles. Short bubbles do not provide the surfactants with sufficient length to adsorb and equilibrate and hence violate the boundary conditions imposed here for semi-infinite bubbles. A simple estimate yields that the dimensionless bubble length scaled by the capillary radius must be greatly in excess of the dimensionless adsorption parameter, the Stanton number $St = k/U$, for boundary condition (2.10) to be valid. Some values of $StCa = k\mu/\gamma_0$ have been measured by Whitaker & Pierson (1976) and Hedge & Slattery to be $StCa \approx 10^{-6}$. Although their conditions are different from the experiments of Schwartz *et al.* (1986), it is still very plausible that, at low Ca, the semi-infinite problem studied here is only valid when the bubble length is many times the capillary radius. In a separate paper (Ratulowski & Chang 1989), we have studied the transport of finite bubbles in capillaries in the absence of Marangoni effects.

For the bulk surfactant transport equations (2.3), the transverse radial boundary conditions are

$$\boldsymbol{n}\cdot\nabla C = 0 \quad \text{on} \quad W, \tag{2.11}$$

$$\frac{1}{Pe}\boldsymbol{n}\cdot\nabla C = -j \quad \text{on} \quad S, \tag{2.12}$$

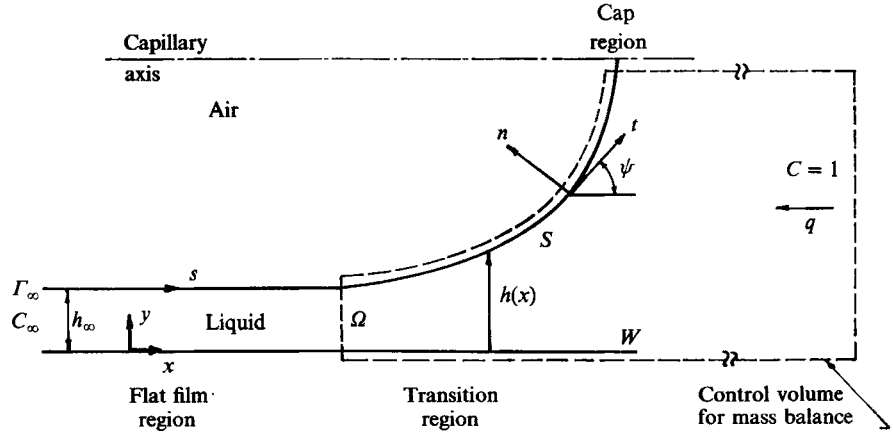

FIGURE 2. Local Cartesian and arclength–angle coordinates travelling at the same speed as the bubble. The control volume shown extends to $x = \infty$ where the bulk concentration is unity and ends to the left at an arbitrary position with liquid flow area Ω. It is bounded by the interface S, the capillary wall W and the capillary axis in the other directions.

where j is the dimensionless flux (scaled by UC_0) to the interface. We shall assume a linear adsorption kinetics of the form

$$j = St(C - \Gamma/K), \tag{2.13}$$

where the Stanton number $St = k/U$ is the adsorption rate constant k scaled by the bubble velocity U and K is the dimensionless adsorption equilibrium constant with proper scaling by the capillary radius R. The axial boundary conditions for C are, assuming the bulk surfactants have equilibrated at $x = -\infty$,

$$C \to 1 \quad \text{as} \quad x \to +\infty, \tag{2.14}$$

$$\frac{\partial C}{\partial x} \to 0 \quad \text{as} \quad x \to -\infty. \tag{2.15}$$

Equation (2.15) indicates that C approaches an unknown equilibrium value C_∞ in the flat-film region. This is consistent with the physical model that this uniform film region is stagnant in the fixed laboratory coordinate and an equilibrium exists between the interfacial and bulk surfactants,

$$\Gamma_\infty \to KC_\infty \quad \text{as} \quad x \to -\infty. \tag{2.16}$$

An additional equation is provided by an overall mass balance as shown in figure 2. Applying the Gauss divergence theorem to the bulk transport equation in the closed volume shown in figure 2 and imposing boundary conditions (2.11) and (2.14), one obtains for every arbitrary transverse cross-section Ω,

$$\int_\Omega \left(\frac{1}{Pe}\frac{\partial C}{\partial x} - uC\right) + q - \frac{1}{Pe}\int_s \boldsymbol{n}\cdot\nabla C = 0, \tag{2.17}$$

where u is the axial velocity component and q is the liquid axial flow rate relative to the moving coordinate in figure 1

$$q = \int_\Omega \boldsymbol{u}\cdot\boldsymbol{n}. \tag{2.18}$$

The quantity q is a constant at every axial position and it is a negative number since the net flow is in the negative x-direction in our moving coordinate. A constant q, however, does not imply a constant flow rate q' in the fixed laboratory frame. In fact, the two are related by

$$q' = q + Ca\,A, \tag{2.19}$$

where A is the area of liquid flow cross-section Ω. The quantity A varies with the axial coordinate x. A similar application of the divergence theorem to the interfacial transport equation (2.4) in the same closed volume yields

$$\frac{1}{Pe}\int_S \boldsymbol{n}\cdot\nabla C = u^\sigma \Gamma|_\Omega, \tag{2.20}$$

which when combined with (2.16) provides the desired condition for Γ,

$$\int_\Omega \left(\frac{1}{Pe}\frac{\partial C}{\partial x} - uC\right) + q - u^\sigma \Gamma = 0, \tag{2.21}$$

at every x position.

The only remaining equation is the relationship between the surface tension γ and the interfacial surfactant concentration Γ. This equation of state is implicitly defined as $\gamma(\Gamma)$.

3. Perturbation analysis of the equations of motion

The governing equations with the free surface S presented in the previous section are too complicated for numerical solution. Numerical attempts on the much simpler surfactant-free problem by finite-difference (Reinelt & Saffman 1985), finite-element (Shen & Udell 1985) and boundary integral (Lu & Chang 1988) techniques have only succeeded in resolving the thin film down to $Ca = 0.5 \times 10^{-3}$ (Lu & Chang 1988). This resolution is certainly inadequate since deviation from Bretherton's theory occurs below $Ca = 10^{-3}$ as seen in figure 8. Consequently, we shall apply a perturbation analysis, similar to that of Park & Homsy (1984) for the surfactant-free problem, to reduce the governing partial differential equations to a more tractable set of lubrication equations which are ordinary differential equations in the axial coordinate x. We begin with the equations of motion in this section and analyse the surfactant transport equations in the next one.

At low Ca, the bubble cap is nearly a static sphere. In the region where the film joins the capillary wall and becomes a flat film, both viscous and capillary forces are important in the momentum transport equations. Since this transition region is very thin, the characteristic length δ in the axial direction is much larger than the characteristic film thickness ϵ in the radial direction. The ratio of these two characteristic lengths is the film number

$$f = \epsilon/\delta \ll 1. \tag{3.1}$$

The dimensionless axial velocity u in the film is $O(1)$ and hence, from the continuity equation (2.2), the radial velocity is $O(f)$. The dimensionless pressure p is also of $O(1)$. Using these order assignments in (2.1), the equations of motion become, to leading order in f, the following lubrication equations

$$Ca\frac{\partial^2 u}{\partial y^2} = \frac{\partial p}{\partial x}, \tag{3.2}$$

$$\frac{\partial p}{\partial y} = 0, \tag{3.3}$$

where y is a local Cartesian coordinate normal to the capillary wall. Because the film is thin and of $O(\epsilon)$, the cylindrical coordinate collapses into a Cartesian one to leading order in f.

The no-slip condition (2.5) remains at

$$u(y=0) = -1, \tag{3.4}$$

and assuming that the surface tension does not vary much from its reference value such that $\gamma = 1 + o(1)$, the normal and tangential stress conditions on S of (2.6) and (2.7) also reduce to (see Ratulowski's thesis for details)

$$p = -h_{xx} - 1 \quad \text{on} \quad S, \tag{3.5}$$

and

$$\frac{\partial \gamma}{\partial x} = Ca \frac{\partial u^\sigma}{\partial y} \quad \text{on} \quad S, \tag{3.6}$$

where the interface S is now defined by the curve $y = h(x)$. Equation (3.6) indicates that the direction of interfacial drag is determined by the direction of the surface tension gradient. Since $p \approx O(1)$, (3.2) and (3.5) stipulate that $\epsilon^2/\delta \approx O(Ca)$ and $\epsilon/\delta^2 \approx O(1)$ for these dominating terms to balance. If these two conditions are not satisfied, there is either no flow or viscous and capillary forces do not balance. These two stipulations then specify the order of δ and ϵ in Ca,

$$\delta \approx O(Ca^{\frac{1}{3}}), \tag{3.7}$$

$$\epsilon \approx O(Ca^{\frac{2}{3}}), \tag{3.8}$$

$$f = \epsilon/\delta \approx O(Ca^{\frac{1}{3}}). \tag{3.9}$$

Hence, for the lubrication equations to be valid, i.e. $f \ll 1$, Ca must be small. The above order assignments are identical to those by Park & Homsy (1984) for the surfactant-free case because we assume $\gamma \approx 1$.

Solving for u in (3.2) with boundary condition (3.4) and the obvious condition $u(y = h) = u^\sigma$, one obtains after imposing (3.3),

$$u(x,y) = \frac{1}{2Ca}\frac{dp}{dx}(y^2 - h(x)\,y) + y(u^\sigma + 1)/h(x) - 1. \tag{3.10}$$

The constant axial flow rate q in the moving coordinate of (2.18) can then be evaluated

$$q = -h_\infty = \int_0^{h(x)} u\,dy = -\frac{1}{12Ca}\frac{dp}{dx}h^3 + \tfrac{1}{2}hu^\sigma - \tfrac{1}{2}h, \tag{3.11}$$

where h_∞ is the thickness of the flat film at $x = -\infty$. It is equal to $-q$ because of the flat velocity profile in the flat film as shown in (2.10). Note that the constant flow rate is always to the left while the interfacial velocity can be either positive or negative.

Substituting the normal stress condition (3.5) into (3.11), one obtains the lubrication equation

$$-\frac{dp}{dx} = \frac{d^3h}{dx^3} = 6Ca[(1-u^\sigma)h - 2h_\infty]/h^3. \tag{3.12}$$

This equation reduces to Bretherton's equation for the surfactant-free mobile case (Bretherton 1961)

$$\frac{d^3h}{dx^3} = 3Ca[h - h_\infty]/h^3, \tag{3.13}$$

under the following two transformations

$$u^\sigma = \tfrac{1}{2}(1-3h_\infty/h), \tag{3.14a}$$

or

$$u^\sigma \to -1, \quad Ca \to \tfrac{1}{4}Ca. \tag{3.14b}$$

We shall show that (3.14*a*) corresponds to the mobile limit of Bretherton's equation while (3.14*b*) actually corresponds to the limit of maximum surfactant effect. For finite surfactant effects, however, the surfactants affect the interfacial velocity u^σ through the Marangoni effect. This requires an expression for the tangential shear or drag τ at the interface S which can be obtained from the lubrication approximation of the axial velocity in (3.10) and the condition (3.11) between q and $\mathrm{d}p/\mathrm{d}x$,

$$\frac{\partial u}{\partial y}(y=h) \equiv \tau(h, u^\sigma) = \left[\frac{4u^\sigma - 2}{h} + \frac{6h_\infty}{h^2}\right]. \tag{3.15}$$

For small variations in γ, the equation of state relating Γ to surface tension $\gamma(\Gamma)$ can be linearized about the unknown tip interfacial concentration Γ_c. The surface tension corresponding to Γ_c is unity owing to our earlier choice of reference surface tension. Hence,

$$\gamma - 1 = \left(\frac{\mathrm{d}\gamma}{\mathrm{d}\Gamma}\right)_c (\Gamma - \Gamma_c) \equiv -Ma(\Gamma - \Gamma_c), \tag{3.16}$$

where Ma is the positive Marangoni number for surfactants. Note that the requirement that $\gamma \approx 1$ implies that $Ma(\Gamma - \Gamma_c)$ is small. For most surfactants, $Ma \approx O(1)$ and $\Gamma - \Gamma_c$ must then be small for the surface tension to vary only slightly and for the lengthscales of (3.7) to (3.9) to be correct. The precise Ca orders of Γ and Γ_c are dependent on the orders of Pe and St as we shall demonstrate in the next section. Substituting (3.16) into (3.6) and invoking (3.15), one obtains a relationship between the interfacial shear Γ and the surface concentration gradient

$$\frac{\mathrm{d}\Gamma}{\mathrm{d}x} = -\frac{Ca}{Ma}\tau(h, u^\sigma), \tag{3.17}$$

where τ is given by (3.15).

Substituting the transformation (3.14*a*) into (3.15) or (3.17), one sees that the interfacial stress τ vanishes everywhere for this particular relationship between u^σ and h. This is also consistent with (3.17) for the limit of zero Marangoni effect $Ma \to 0$. In this mobile limit, the limiting interfacial velocity of the bubble cap region is $u^\sigma_{\lim} = 0.5$ to leading order since in (3.14*a*) $h_\infty/h \approx \epsilon \approx O(Ca^{\frac{2}{3}}) \ll 1$ in the cap region. This mobile cap interfacial velocity is positive while the interfacial velocity in the flat film region is negative at -1 from (2.10). The sign reversal occurs at a stagnation point in the moving frame at $h = 3h_\infty$ which has been confirmed by the numerical solutions of Reinelt & Saffman (1985) and Lu & Chang (1988) of the full Stokes problem.

Another interesting result of (3.17) is that as $Ca/Ma \to \infty$, the interfacial shear τ vanishes and one obtains the mobile expression for u^σ in (3.14*a*). Consequently, at sufficiently large Ca (but still small enough for the lubrication approximation to be valid), the traction τ caused by the Marangoni effect of surface concentration gradient becomes negligible and the mobile results of Bretherton should be approached. As seen in figure 8, this is observed in all reported experiments. We shall obtain the proper parameter orders for this mobile limit in the next section.

Equations (3.12) and (3.17) represent the lubrication approximations of the equations of motion and the interfacial conditions. They remain incomplete since

$u^{\sigma}(x)$ is still unknown and must be derived from a similar lubrication analysis of the surfactant transport equations. The corresponding perturbation analysis is more involved owing to the widely varying orders of Pe and St, representing the ratios of diffusion and adsorption timescales to the axial convection timescale. In carrying out this analysis, we shall impose the conditions $\gamma \approx 1$ and only trace amounts of surfactant exist on the interface, $\Gamma \approx \Gamma_c \ll 1$, for consistency.

Before we carry out a perturbation analysis of the surfactant equations, we shall examine the momentum equation in the static cap region. The solution $h(x)$ to the lubrication equations (3.12) and (3.17) must merge into this static cap. In this region, viscous effects are negligible since both the axial and radial lengthscales are of $O(1)$ and hence, to leading order, the left-hand side of (2.1) vanishes and p is a constant. The tangential stress condition (2.7) and the linearized equation of state (3.16) also imply that Γ and γ approach asymptotically their values at the tip, Γ_c and unity, respectively. (The quantity Γ_c is unknown and must be obtained from the computations.) Hence, the normal stress condition (2.6) implies that the surface in the cap region is governed by the constant curvature Laplace–Young equation

$$p = -\kappa, \tag{3.18}$$

where κ is the full curvature expression

$$\kappa = \frac{h_{xx}}{(1+h_x^2)^{\frac{3}{2}}} + \frac{1}{(1+h_x^2)^{\frac{1}{2}}(1-h)}, \tag{3.19}$$

and the first term is the axial curvature while the second the azimuthal curvature. In the transition region $\kappa \approx h_{xx}+1 \approx O(1)$ since $h_x \approx O(f) = O(Ca^{\frac{1}{3}})$. This result is employed in (3.5). However, in the cap region, $h_{xx} \approx h_x \approx O(1)$ and the full expression must be used.

The profile $h(x)$ from the transition region must match into the constant curvature spherical surface in (3.18). This matching is classically done by the method of matched asymptotic expansion (Park & Homsy 1984). However, as Wilson (1982) has suggested for the plate drag-out problem, if one relates p to the full curvature (3.19) in the lubrication equation of (3.12) instead of the lubrication approximation of (3.5), all terms which are important in both the transition and static cap regions are included. Moreover, both (3.12) and (3.18) are approached in the proper lubrication limit of $x \approx \delta \approx O(Ca^{\frac{1}{3}})$ and $y \approx h \approx \epsilon \approx O(Ca^{\frac{2}{3}})$ and the static limit of $x \approx y \approx O(1)$. This composite equation can be integrated through both the transition region and the cap region with the matching occurring internally. The numerical integration is made even simpler if one introduces the arclength–angle coordinate in figure 1 to avoid the singularity of $h(x)$ at the tip. This technique has been applied by Goldshtik, Khanin & Ligai (1986) and Secomb & Skalak (1982) for other lubrication flows. The arclength–angle coordinates are

$$\mathrm{d}x = \cos\psi\,\mathrm{d}s, \quad \mathrm{d}y = \sin\psi\,\mathrm{d}s, \tag{3.20a, b}$$

such that the composite form of the lubrication equations (3.12) and (3.17) become

$$\frac{\mathrm{d}p}{\mathrm{d}s} = -6Ca\cos\psi[(1-u^{\sigma})h - 2h_{\infty}]/h^3, \quad \frac{\mathrm{d}\psi}{\mathrm{d}s} = -p - \frac{\cos\psi}{1-h}, \tag{3.21a, b}$$

$$\frac{\mathrm{d}h}{\mathrm{d}s} = \sin\psi, \quad \frac{\mathrm{d}\Gamma}{\mathrm{d}s} = -\cos\psi\,\frac{Ca}{Ma}\tau(h, u^{\sigma}), \tag{3.21c, d}$$

The term $d\psi/ds$ in the normal stress condition (3.21*b*) is the axial curvature while $\cos\psi/(1-h)$ is the azimuthal curvature in the arclength–angle coordinates. At the tip, both curvatures approach unity. Although one cannot scale away Ca and h_∞ in (3.21) as in Bretherton's analysis for the mobile limit, we have shown that (3.21), which is an autonomous dynamical system, is much more amenable to a numerical shooting scheme from the flat film to the cap (Ratulowski & Chang 1989). In the present surfactant case, only a few parameters can be scaled away in some limiting conditions and the above arclength–angle formulation of the composite equation seems to be the only feasible way of matching the lubrication solutions to the static cap.

By stipulating that capillary forces balance viscous forces, the film is thin and $\Gamma \approx \Gamma_c \ll 1$, we have obtained the order assignments of the axial and transversal characteristic lengths in (3.7) and (3.8) from the equations of motion. Surfactant effects on these lengthscales are removed by assuming that the surface tension does not vary significantly. However, since the film thickness is only of $O(Ca^{\frac{2}{3}})$, this small variation in surface tension can cause the thickness to increase by factors of $O(1)$. Larger-order increases by the Marangoni effect would violate the order assignments of (3.7) and (3.8). Fortunately, except for the low Ca data of Chen in figure 8, the observed increase is never more than a factor of 3. This confirms our low-surfactant-concentration assumption, $\Gamma \ll 1$.

4. Perturbation analysis of surfactant transport

The lubrication equations of (3.12) and (3.17) or the composite equations of (3.21) must be complemented by the surface and bulk transport equations of the surfactants in (2.3), (2.4) and (2.17). These equations can also be simplified into ordinary differential equations in the axial coordinate x or the arclength s, such as (3.21), if the bulk concentration C is independent of the transverse radial coordinate r or its local Cartesian counterpart y. In the local Cartesian coordinate, the bulk transport equation (2.3) becomes

$$u\frac{\partial C}{\partial x}+v\frac{\partial C}{\partial y}=\frac{1}{Pe}\left(\frac{\partial^2 C}{\partial x^2}+\frac{\partial^2 C}{\partial y^2}\right). \tag{4.1}$$

Imposing the x and y lengthscales of (3.7) and (3.8) in the transition region, which have been dictated by viscous and capillary forces, and the velocity scales from the continuity equation, one concludes that radial diffusion dominates over convection only if the transverse diffusive characteristic time $R^2\epsilon^2/D$ is much smaller than the convective characteristic time $R\delta/U$. (Note that radial diffusion is always faster than axial diffusion because of the shorter transverse characteristic length ϵ in the transition region as dictated by the balance of viscous and capillary forces in (3.7) and (3.8).) Hence, one obtains the following condition for radial diffusion to dominate

$$Pe \ll Ca^{-1}. \tag{4.2}$$

Typical Péclet numbers of surfactants in 100 μm capillaries are about $10^5\,Ca$ (assuming a diffusivity of 10^{-5} cm^2/s). Hence, at low $Ca\,(<10^{-3})$, (4.2) is always satisfied. Condition (4.2) then stipulates that (4.1) reduces to $\partial^2 C_0/\partial y^2 = 0$ where C_0 is the leading-order expansion of C. The no-flux boundary condition at the wall of (2.11) then stipulates that C_0 is independent of the radial direction. Consequently, to

leading order, bulk transport of surfactants is described by the overall balance of (2.21) which simplifies to

$$\frac{\mathrm{d}C_0}{\mathrm{d}x} = \frac{Pe}{h}[u^\sigma \Gamma - q + qC_0] = \frac{Pe}{h}[u^\sigma \Gamma + h_\infty - h_\infty C_0], \tag{4.3}$$

where (2.18) has been used.

The order assignment of the interfacial concentration can now be made explicit from (4.3). Requiring that interfacial flux must balance bulk flux and noting that C_0 and u^σ are both order unity, one concludes that Γ is the same order as h_∞,

$$\Gamma \approx O(Ca^{\frac{2}{3}}). \tag{4.4}$$

Hence, for all our order assignments to be valid, including the ones involved in the momentum lubrication analysis, we are restricted to trace amounts of impurities. This is the case in all experiments in figure 8 where an $O(Ca^{\frac{2}{3}})$ variation in Γ and surface tension gradient $\mathrm{d}\gamma/\mathrm{d}x$ cause an order unity correction to the $O(Ca^{\frac{2}{3}})$ film thickness h_∞. Some experiments (Hirasaki & Lawson 1985), however, introduce large amounts of surfactants at concentrations above the critical micelle concentration. Our analysis would not apply to these experiments.

The bulk balance equation of (4.3) includes both axial diffusion and convection. We can now assign the relative importance of these two mechanisms while still requiring (4.2) such that radial diffusion is faster than both,

$$Pe \approx O(Ca^0) \text{ or smaller} \quad \text{axial diffusion} \gg \text{convection}, \tag{4.5a}$$

$$Pe \approx O(Ca^{-\frac{1}{3}}) \quad \text{axial diffusion} \approx \text{convection}, \tag{4.5b}$$

$$Pe \approx O(Ca^{-\frac{2}{3}}) \quad \text{axial diffusion} \ll \text{convection}. \tag{4.5c}$$

These assignments allow further simplification of (4.3).

In the flat-film region, imposing the flat velocity profile of (2.10) and the equilibrium conditions of (2.15) and (2.16) on (4.3) then yields

$$C_\infty = h_\infty/(1+Kh_\infty), \quad \Gamma_\infty = KC_\infty, \tag{4.6a, b}$$

which shall be used as boundary conditions at $-\infty$ for our transport equations.

Although there is only a trace amount of surfactants on the interface according to (4.4), they must still satisfy the surface transport equations of (2.4) and (2.12). To leading order in the transition region, these equations become

$$\frac{\mathrm{d}}{\mathrm{d}x}(u^\sigma \Gamma) = St(C_0 - \Gamma/K). \tag{4.7}$$

Imposing the appropriate orders for each variable in (4.7), we see that convection on the left-hand side balances adsorption on the right-hand side if

$$St \approx O(Ca^{\frac{1}{3}}). \tag{4.8}$$

If St is lower order than $Ca^{\frac{1}{3}}$, then there is no adsorption and one returns to Bretherton's mobile theory. However, if St is larger order than $Ca^{\frac{1}{3}}$, indicating fast adsorption, a local equilibrium exists between the bulk and surface surfactants,

$$\Gamma = KC_0. \tag{4.9}$$

Typical values of $StCa = k\mu/\gamma_0$ can be estimated from the work of Whitaker & Pierson (1976) and Hedge & Slattery (1971) to be $StCa \approx 10^{-6}$. Consequently, St is $O(1)$ at low Ca.

Based on the above order estimates on Pe and St, we have constructed the following models with different degrees of axial diffusion, convection and adsorption resistance,

$$Pe \approx Ca^{-\frac{2}{3}} \quad St \approx 1 \quad \text{convective-equilibrium model,} \tag{4.10a}$$

$$Pe \approx Ca^{-\frac{1}{3}} \quad St \approx 1 \quad \text{diffusive-equilibrium model,} \tag{4.10b}$$

$$Pe \approx Ca^{-\frac{2}{3}} \quad St \approx Ca^{\frac{1}{3}} \quad \text{convective-adsorption model,} \tag{4.10c}$$

$$Pe \approx Ca^{-\frac{1}{3}} \quad St \approx Ca^{\frac{1}{3}} \quad \text{diffusive-adsorption model,} \tag{4.10d}$$

$$Pe \approx Ca^{0} \quad St \approx Ca^{\frac{1}{3}} \quad \text{bulk equilibrium model.} \tag{4.10e}$$

The first part of each title indicates whether bulk convection is as important as bulk axial diffusion while the second part indicates whether adsorption is fast enough for interfacial convection to be neglected and a local equilibrium established. The bulk equilibrium model represents the limit of fast diffusion in the bulk such that the bulk concentration is gradientless. Interfacial convection, however, remains important in this model. Otherwise there would be no surfactant concentration gradient at all. Within these ranges of Pe and St, the bulk balance equation of (4.3) and the interfacial transport equation of (4.7) reduce to the following forms:

(a) convective-equilibrium

$$C_0 = 1+(u^\sigma\Gamma/h_\infty), \quad C_0 = \Gamma/K, \tag{4.11a, b}$$

(b) diffusive-equilibrium

$$\frac{\mathrm{d}C_0}{\mathrm{d}x} = \frac{Pe}{h}[u^\sigma\Gamma+h_\infty-h_\infty C_0], \quad C_0 = \Gamma/K, \tag{4.12a, b}$$

(c) convective-absorption

$$C_0 = 1+(u^\sigma\Gamma/h_\infty), \quad \frac{\mathrm{d}}{\mathrm{d}x}(u^\sigma\Gamma) = St\left(1+\frac{u^\sigma\Gamma}{h_\infty}-\frac{\Gamma}{K}\right), \tag{4.13a, b}$$

(d) diffusive-adsorption

$$\frac{\mathrm{d}C_0}{\mathrm{d}x} = \frac{Pe}{h}[u^\sigma\Gamma+h_\infty-h_\infty C_0], \quad \frac{\mathrm{d}}{\mathrm{d}x}(u^\sigma\Gamma) = St(C_0-\Gamma/K), \tag{4.14a, b}$$

(e) bulk equilibrium

$$C_0 = 1, \quad \frac{\mathrm{d}}{\mathrm{d}x}(u^\sigma\Gamma) = St(1-\Gamma/K). \tag{4.15a, b}$$

All the models can be derived from the diffusive-adsorption model of (4.14) by taking limits of zero Pe, infinite Pe or infinite St according to the hierarchy in figure 3.

From (4.11)–(4.15), one can obtain two equations, which may be algebraic equations or first-order differential equations, for C_0 and u^σ. (Some manipulation is necessary for models (c)–(e).) These two surfactant transport equations can then be coupled to the momentum lubrication equations of (3.12) and (3.17) to form a complete set of equations. This set of equations can also be formulated as composite equations for numerical matching to the constant curvature cap region. It would be extremely difficult to carry out the matching with the lubrication equations of (3.12)

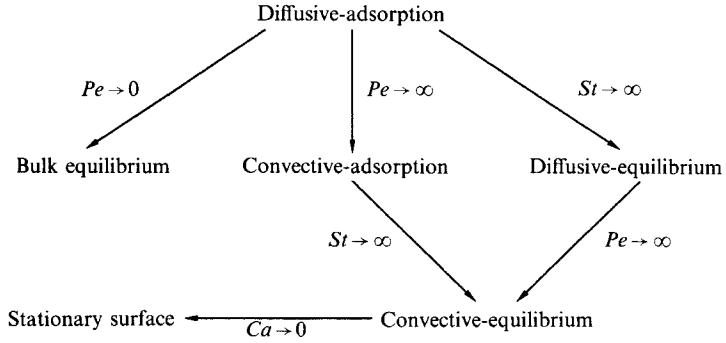

FIGURE 3. Hierarchy of the models for various order of Péclet and Stanton numbers. All models can be reduced from the diffusive-adsorption model. All but the bulk equilibrium model reduce to the convective-equilibrium model.

and (3.17) as Bretherton has done for the mobile case. As an example, the diffusive-adsorption model equations in the arclength–angle formulation are

$$\frac{dp}{ds} = -6Ca\cos\psi[(1-u^\sigma)h - 2h_\infty]/h^3, \tag{4.16a}$$

$$\frac{d\psi}{ds} = -p - \cos\psi/(1-h), \tag{4.16b}$$

$$\frac{dh}{ds} = \sin\psi, \tag{4.16c}$$

$$\frac{du^\sigma}{ds} = \cos\psi\left\{\frac{Ca}{Ma}u^\sigma\tau/\Gamma - St\left(\frac{1}{K} - \frac{C_0}{\Gamma}\right)\right\}, \tag{4.16d}$$

$$\frac{dC_0}{ds} = Pe\{u^\sigma\Gamma - h_\infty(C_0-1)\}\cos\psi/h, \tag{4.16e}$$

$$\frac{d\Gamma}{ds} = -Ca\,\tau\cos\psi/Ma, \tag{4.16f}$$

where the interfacial shear expression $\tau(h, u^\sigma)$ is given by (3.15). Equations (4.16) is a sixth-order autonomous system of ordinary differential equations with the arclength s as the independent variable. The parameters are Ca, Ma, St and Pe. The unknown film thickness h_∞ is determined by matching the solutions to certain boundary conditions at the tip which will be clarified in the next section. Note that u^σ, C_0, Γ and p all approach asymptotic limits near the tip ($\psi = \frac{1}{2}\pi$). While there are no stipulations on the limiting values of u^σ, Γ and p at the cap, boundary condition (2.14) stipulates a far-field concentration for C upstream. The limiting value C_0 at the tip, C_c, will be different from unity in general and to trace the bulk concentrate profile beyond the bubble tip, one simply integrates an equivalent form of (4.4) without the interface S,

$$\frac{1}{Pe}\frac{\partial C_0}{\partial x} = q(C_0-1) = h_\infty(1-C_0), \tag{4.17}$$

from the tip to $x \to \infty$. The concentration is then ensured to approach unity far upstream. Equation (4.17) requires that radial diffusion remains dominant over axial diffusion and convection in front of the tip such that $C \approx C_0(x)$. It, however, does not

require the flow field to be approximately unidirectional near the tip since (2.17) and (4.3) are applicable to two-dimensional flow fields if C is independent of y.

Whether the models in (4.11)–(4.15) will lead to a thicker film is governed by the surfactant transport equations. If the traction τ is negative throughout the entire transition region as indicated in figure 1, then the net flow rate into the film will be larger than the mobile case and a thicker film is produced. A negative τ along the interface, from the interfacial shear expression of (3.17), implies a monotonically increasing interface concentration from the film to the cap $\mathrm{d}\Gamma/\mathrm{d}x > 0$. It is hence sufficient to show that the interface concentration gradient is positive for a positive correction to Bretherton's mobile film thickness. There are several mechanisms which determine the distribution of interfacial surfactants. Consider the general interfacial transport equation (4.7) of the diffusive-adsorption equation. It can be rewritten as

$$\frac{\mathrm{d}\Gamma}{\mathrm{d}x} = -\frac{\Gamma}{u^\sigma}\frac{\mathrm{d}u^\sigma}{\mathrm{d}x} + \frac{St}{u^\sigma}(C_0 - \Gamma/K). \tag{4.18}$$

The first term on the right-hand side is due to surface dilation where $\mathrm{d}u^\sigma/\mathrm{d}x$ is positive as the cap moves away from the stationary film in the fixed laboratory frame. The second term describes the adsorption of surfactants from the bulk to the interface. Whether these terms will contribute to a positive surfactant gradient on the interface depends on the sign of u^σ. Recall from (3.14a) that for Bretherton's mobile case, a stagnation point in the moving frame, where u^σ vanishes, exists at $h = 3h_\infty$. Depending on the net effect of the traction τ, this stagnation point may move away or closer to the flat film. Consider first the left-hand side of the stagnation point where u^σ is negative and the adsorption term favours a negative interfacial gradient. Physically, the interface is picking up surfactants from the bulk as it moves to the left. The contribution of this mechanism can be diminished if the bulk concentration C_0 decreases downstream, hence reducing the adsorption rate. The same argument holds on the right-hand side of the stagnation point where the adsorption term favours a positive $\mathrm{d}\Gamma/\mathrm{d}x$ since u^σ is positive. In this case, a positive $\mathrm{d}C_0/\mathrm{d}x$ also would favour a positive interfacial gradient. These physical arguments then indicate that a positive bulk concentration gradient favours a thicker film. Since this is not present in the bulk equilibrium model, a thinner film may result as there is no mass-transfer resistance in the bulk. Indeed, a perturbation analysis in St by Ginley & Radke (1989) indicates that the bulk equilibrium model does predict a small reduction in film thickness, contrary to the data in figure 8. The above arguments, however, suggest that the convective-equilibrium model, where a bulk gradient exists and the unfavourable surface convection is negligible relative to adsorption, may produce a thicker film. This can indeed be rigorously shown. Eliminating C_0 from the two transport equations in (4.11) yields a relationship between interfacial velocity and concentration

$$u^\sigma = h_\infty\left(\frac{1}{K} - \frac{1}{\Gamma}\right). \tag{4.19}$$

Substituting (4.19) into the interfacial shear–concentration relationship of (3.17) yields

$$\frac{\mathrm{d}u^\sigma}{\mathrm{d}x} = -h_\infty\frac{Ca}{Ma}\left(\frac{1}{K} - \frac{u^\sigma}{h_\infty}\right)^2\tau(h, u^\sigma). \tag{4.20}$$

This then implies that τ is negative throughout the transition region because $\mathrm{d}u^\sigma/\mathrm{d}x$ is positive owing to the dilation of the surface as the cap moves away from the station film. Hence, the convective-equilibrium model predicts a thicker film. A simple

manipulation of (4.19) and (4.11*b*) also confirms that both C_0 and Γ increase monotonically from the flat film to the cap.

From (4.20) of the convective-equilibrium model, an estimate of when Bretherton's mobile limit is approached ($\tau \to 0$) can be obtained. From (3.15), τ is of order $h_\infty^{-1} \approx Ca^{-\frac{2}{3}}$. Imposing this order and the appropriate orders of $u^\sigma \approx O(1)$ and $x \approx O(Ca^{\frac{1}{3}})$ from the momentum equations, one concludes from (4.20) that the mobile limit is reached if Ca/MaK^2 is $O(Ca^{-\frac{2}{3}})$ or larger. If K and Ma are fixed, then the mobile limit is reached when Ca is in excess of

$$Ca^* \approx Ma^{\frac{3}{5}}K^{\frac{6}{5}}. \tag{4.21}$$

Hence, a higher K, implying a higher affinity for the surface species, requires a higher Ca^* before the mobile limit can be achieved. This is consistent with the data of figure 8 which show that water has a higher Ca^* than benzene and aniline. Surfactants have a higher affinity for the air–water interface because their non-polar hydrocarbon tail is rejected by water and protrudes into the air phase. Benzene and aniline do not reject the hydrocarbon tail as much and the surfactants do not favour the interface with equal affinity. A larger Ma also implies that a higher Ca must be reached before the Marangoni effect becomes negligible.

The opposite limiting case occurs when surface dilation $\mathrm{d}u^\sigma/\mathrm{d}x$ vanishes exactly and the interface approaches a stationary interface. By imposing the appropriate orders for the terms in (4.20), one concludes that this stationary surface limit occurs when Ca/MaK^2 is of order unity. If Ma and K are fixed, then this limit is approached when Ca is less than

$$Ca_* \approx MaK^2. \tag{4.22}$$

If surface dilation does not occur, boundary condition at the flat-film region requires that $u^\sigma = -1$ everywhere, viz. the interface is stationary in the laboratory coordinate. This is not the constant-shear rigid model of Bretherton and Goldsmith & Mason because the interface is not being dragged. Even though the interface is stationary, the fluid below it is still flowing owing to the pressure gradient except in the flat-film region. More importantly, the interfacial shear in this limit

$$\tau(h) = 6(h_\infty/h - 1)/h, \tag{4.23}$$

vanishes in the flat film $h = h_\infty$ which is not true of the rigid models. This limit is a singular one since the tip velocity cannot be -1. However, we shall show in later integrations of the full equation that this stationary surface model does correctly predict the limiting film thickness for large K and at low Ca. In this limit, the surfactant equations are decoupled from the equations of motion since u^σ is known. Returning to the momentum lubrication equations of (3.12) and replacing u^σ by -1 yield an equation that can be transformed to the Bretherton equation of (3.13) by transformation (3.14*b*). Consequently, the mobile results of Bretherton

$$h_\infty = 1.3375\,Ca^{\frac{2}{3}}, \quad \Delta p = 9.40\,Ca^{\frac{2}{3}}, \tag{4.24a, b}$$

can be easily extended to provide the maximum increase due to Marangoni effect. In (4.24*b*), Δp is the pressure drop across the entire bubble. Using transformation (3.14*b*), the maximum increases in film thickness and pressure drop relative to Bretherton's mobile limit are then

$$\nu_h = \nu_p = 4^{\frac{2}{3}} = 2.52, \tag{4.25}$$

where ν_h and ν_p refer to the film thickness and pressure drop of the stationary surface model relative to Bretherton's mobile result. These corrections of Bretherton's

mobile result in (4.25) for the stationary surface limit can be approached by lowering Ca or increasing Ma or K such that Ca/MaK^2 is of $O(1)$. As is evident in figure 8, they bound most measurements except the low Ca data of Chen. As Chen has indicated, longitudinal surface grooves on his capillaries are probably responsible for a constant low Ca tail of his data, which is the portion not bounded by (4.25). His constant tail corresponds to the average depth of the grooves which is much larger than the overlying film thickness at low Ca. Data of other experiments do not show these tails and they all approach the mobile limit at high Ca and the stationary surface limit at low Ca. As stated, the relative closeness to these two envelopes for different liquid–water systems is also consistent with their values of K and Ma. In between the two envelopes, which vary as $Ca^{\frac{2}{3}}$, the experimental curves have a smaller exponent dependence on Ca. Fairbrother & Stubbs have shown that the film thickness of their water–air system varies as $Ca^{\frac{1}{2}}$. In the next section, we investigate this intermediate behaviour between Ca_* and Ca^*. We shall also study the most sophisticated model, the diffusive-adsorption model to scrutinize the effect of bulk diffusion which is neglected in the convective-equilibrium model.

5. Integration of the lubrication equations

The composite equations for the convective-equilibrium model can be constructed by casting (4.20) in the arclength–angle coordinated and by coupling the resulting equations to the composite momentum equations

$$\frac{\mathrm{d}p}{\mathrm{d}s} = -6Ca\cos\psi[(1-u^\sigma)h - 2h_\infty]/h^3, \quad \frac{\mathrm{d}\psi}{\mathrm{d}s} = -p - \cos\psi/(1-h), \quad (5.1a, b)$$

$$\frac{\mathrm{d}h}{\mathrm{d}s} = \sin\psi, \quad \frac{\mathrm{d}u^\sigma}{\mathrm{d}s} = -h_\infty \frac{Ca}{Ma}\left(\frac{1}{K} - \frac{u^\sigma}{h_\infty}\right)^2 \tau(h, u^\sigma)\cos\psi. \quad (5.1c, d)$$

This is a four-dimensional dynamical system with an unknown parameter h_∞. Five conditions are then necessary to specify the trajectory of (5.1) in the four-dimensional state space which corresponds to the true solution. One condition is that the trajectory must begin from the flat-film region which is a fixed point to (5.1)

$$\begin{pmatrix} p \\ \psi \\ h \\ u^\sigma \end{pmatrix} = \begin{pmatrix} \dfrac{1}{1-h_\infty} \\ 0 \\ h_\infty \\ -1 \end{pmatrix}. \quad (5.2)$$

This corresponds to one and not four conditions because at (5.2) the system remains at the fixed point, which is a static cylinder, without initiating a trajectory. As is typically done in related problems (Bretherton 1961; Wilson 1982), one must perturb the dynamical system slightly away from the fixed point. In the neighbourhood of the fixed point, the trajectory depart the fixed point along the unstable eigenvectors. In Bretherton's mobile problem, there is only one unstable eigenvector and there is no ambiguity about how the interface departs the flat-film region. The eigenvalue problem is different here. In fact, an additional eigenvalue is introduced by surface-tension gradient. If there are multiple unstable eigenvectors, different initial conditions will then lead to different departures from the flat-film fixed point and an elaborate iteration procedure must be implemented to choose the correct direction of

departure. It is hence important to determine the number of unstable eigenvalues to fixed-point (5.2). Linearizing (5.1) about (5.2), one obtains the characteristic polynomial for the eigenvalues,

$$\eta\lambda^4+4\lambda^3-12Ca(4+\eta\lambda)/h_\infty^3+36Ca/h_\infty^3=0, \tag{5.3}$$

where

$$\eta = Ma/Ca\left(\frac{1}{K}+\frac{1}{h_\infty}\right)^2. \tag{5.4}$$

In the limit of Ma or η approaching zero, we recover the three mobile eigenvalues of Bretherton

$$\lambda_1 = (3Ca)^{\frac{1}{3}}/h_\infty, \quad \lambda_{2,3} = -(3Ca)^{\frac{1}{3}}[1\pm\sqrt{3}\mathrm{i}]/2h_\infty, \tag{5.5a, b}$$

where λ_1 is real and unstable and λ_2 and λ_3 are a stable complex pair. A perturbation analysis of (5.3) at small η yields the additional eigenvalue due to the Marangoni effect

$$\lambda_4 \sim -4/h_\infty\eta, \tag{5.6}$$

which is also real and stable. We have found numerically that λ_4 remains real and negative for all values of η and Ca considered. Hence, the presence of surfactant adds a real and stable eigenvalue to the spectrum. The trajectory that leaves the fixed point must not have any contribution from the stable eigenvectors. This constitutes three extra conditions since there are three stable eigenvectors. Integration cannot be initiated with an arbitrary initial condition since any small perturbation away from the fixed point would rapidly converge to the only unstable eigenvector. The trajectory following this unstable eigenvector in the neighbourhood of the fixed point rapidly loses its linearity in the state space as it departs from the fixed point. It soon becomes a curved trajectory known as an unstable invariant manifold in dynamics system theory. This trajectory is required to be tangent to the plane

$$\psi = \tfrac{1}{2}\pi \quad h = 1, \tag{5.7}$$

in the four-dimensional phase space. Condition (5.7) is simply the symmetry condition for the bubble profile at the tip. This condition is the fifth condition required to fully specify the problem.

Numerically, the construction of the unstable manifold for (5.1) from the fixed point (5.2) till tangency with the plane (5.7) is a one-dimensional shooting problem. The parameter h_∞ can be iterated until tangency is achieved. We use a standard Newton iteration technique in conjunction with a fourth-order predictor–corrector method to integrate (5.1). The computed film thickness and liquid pressure at the tip are shown as functions of Ca for two values of Ma and several values of K in figures 4 and 5. The bottom curve is Bretherton's mobile limit of (4.24) corresponding to $K\rightarrow 0$. Since surfactants are not adsorbed onto the interface in this limit, a surface traction does not exist. The top curve corresponds to the stationary surface limit as K approaches infinity. From the order assignment of Γ in (4.4) and the equilibrium relationships of (4.6b) or (4.9), this actually corresponds to $K \gg O(Ca^{\frac{2}{3}})$. At this limit, maximum adsorption of the trace impurities occurs. As was predicted by the asymptotic analysis, all curves enveloped by these two limits approach the mobile limit as Ca exceeds Ca^* of (4.21) and approach the stationary surface limit for Ca less than Ca_* in (4.22). At extremely low Ca values, the maximum correction of $4^{\frac{2}{3}}$ in (4.25) is also obtained. This can also be achieved at relatively high Ca by increasing Ma as shown in figure 6 for $Ca = 1.0\times10^{-4}$ and $K = 0.1$. In between the two limits, the curves vary approximately as aCa^b where b is less than $\frac{2}{3}$ and the proportionality constant a varies with K. Fairbrother & Stubbs have indicated that their air–water

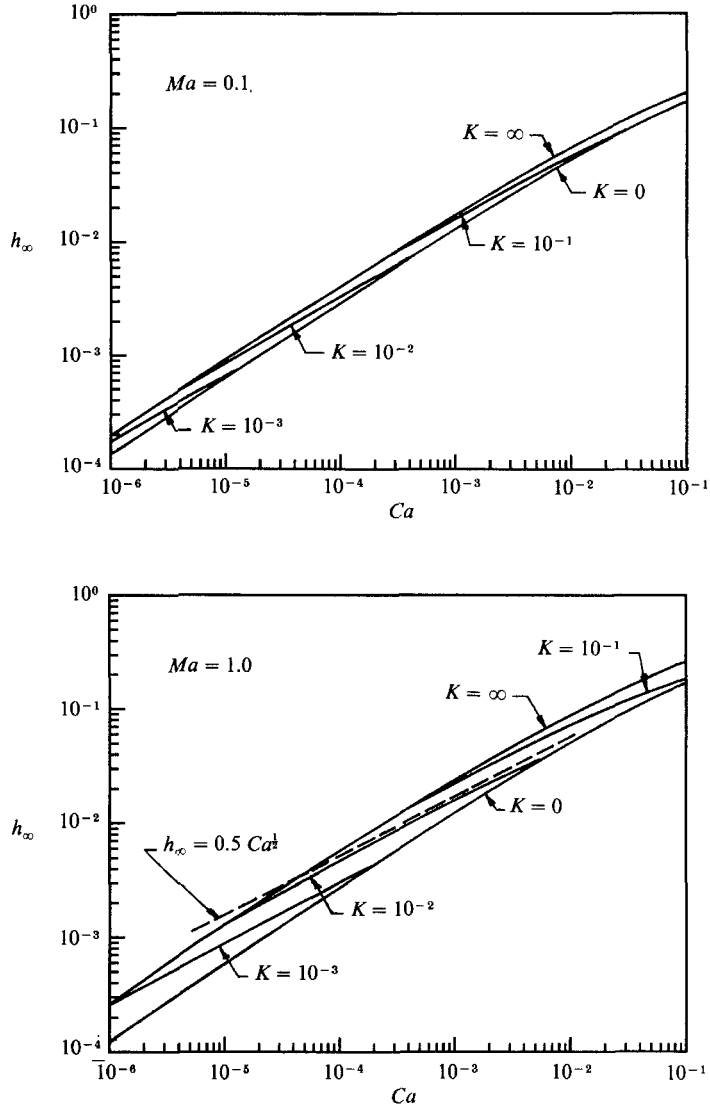

FIGURE 4. Computed film thickness from the convective-equilibrium model for two Marangoni numbers, $Ma = 0.1$ and 1.0. Fairbrother & Stubbs' correlation is also overlayed on the $Ma = 1.0$ curves.

data can be described by $h_\infty = 0.5Ca^{\frac{1}{2}}$ for $7.5 \times 10^{-5} < Ca < 0.014$. As shown in figure 4(*b*), this correlation lies very close to our computed curve for $Ma = 1.0$ and $K = 10^{-2}$. Although data on Ma and K are difficult to obtain even for the air–water system, it is likely that these numbers are close to the actual values since two sets of air–water data measured by Schwartz *et al.* (1986) also lie close to this curve as shown in figure 8.

We demonstrate that the interfacial shear τ is always negative for this model by computing $u^{\sigma}_{\rm lim}$, the limiting interfacial velocity as the stable bubble cap is approached. Recall that the mobile limit of Bretherton's theory in (3.14*a*) yields $u^{\sigma}_{\rm lim} \approx 0.5$ to leading order in Ca. A negative traction would then reduce $u^{\sigma}_{\rm lim}$ from 0.5. Note that the tip velocity should be zero by symmetry. However, the lubrication

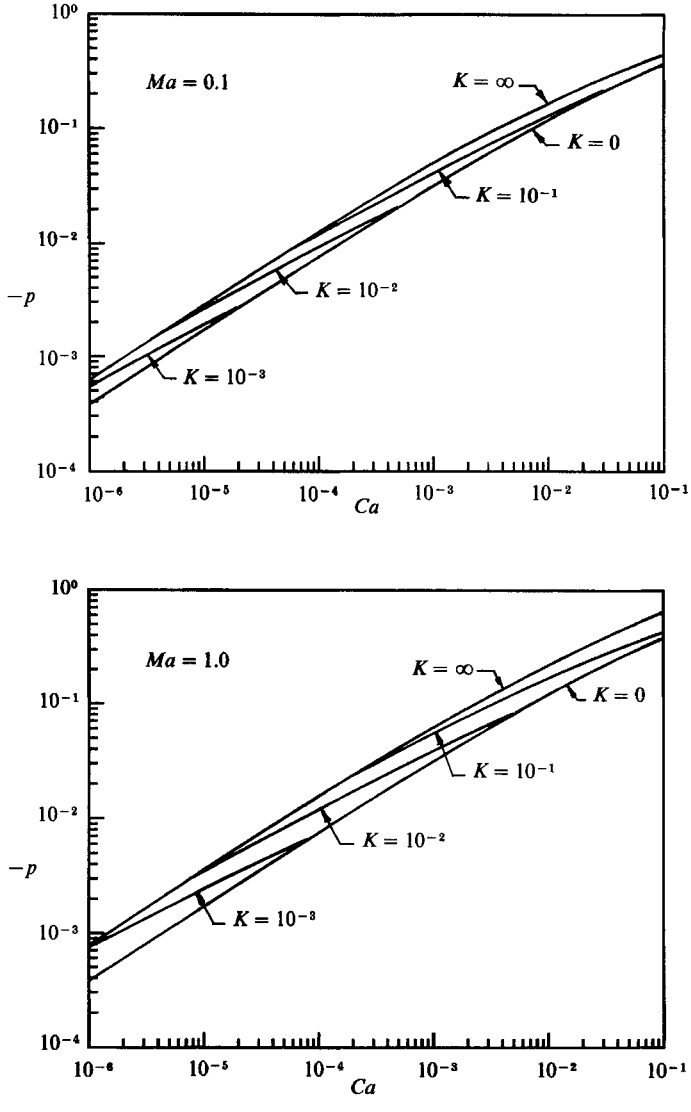

FIGURE 5. Computed liquid pressure at the bubble tip for $Ma = 0.1$ and 1.0.

analysis is not valid exactly at the tip and $u^{\sigma}_{\mathrm{lim}}$ is the limiting interfacial velocity as the static cap region is approached from the transition region. In figure 7, the Bretherton result for $u^{\sigma}_{\mathrm{lim}}$ is the top curve with $K = 0$. As K increases, representing increasing Marangoni effect, $u^{\sigma}_{\mathrm{lim}}$ decreases towards the lower envelope in figure 7 with $K = \infty$. As Ma also increases, this lower envelope decreases towards -1 for all Ca, indicating that maximum surfactant effect is felt when the interface in the transition region becomes stationary in the laboratory frame. For the mobile case, the interfacial velocity in the laboratory frame increases from zero in the flat film to 1.5 as the static cap region is approached at low Ca. Clearly, more flow in the downstream direction occurs when the Marangoni effect becomes appreciable.

Finally, we overlay the $Ma = 1.0$ curves of figure 4 (b) on all available experimental data in figure 8. Although only the parameters Ma and K are free for adjustment and they are selected at convenient values without empirical fitting, surprising

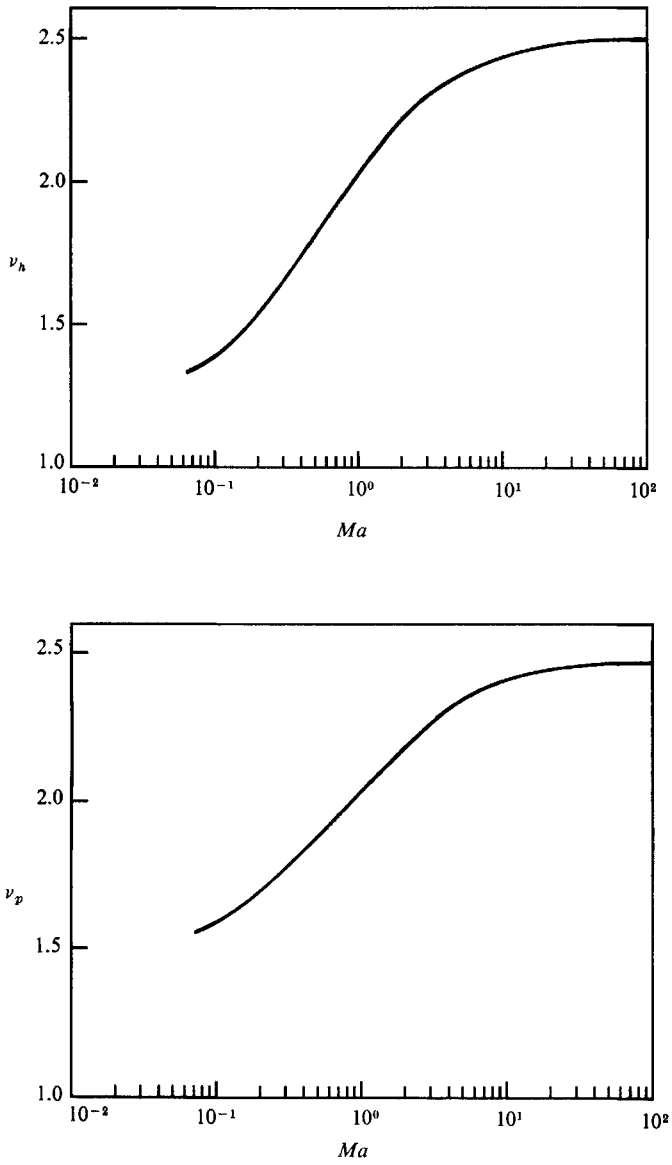

FIGURE 6. The ratio of film thickness ν_h and cap liquid pressure ν_p to the mobile values obtained by Bretherton. An asymptotic approach to the maximum limit of $4^{\frac{2}{3}}$ is observed at large Ma. The parameters are $Ca = 1.0 \times 10^{-4}$ and $K = 0.1$.

quantitative agreement is observed. For example, entire families of data for benzene by Bretherton and for water by Schwartz *et al.* lie on the computed curves for $K = 10^{-3}$ and 10^{-2}, respectively. That the data for water are better described by a higher value of K is also consistent with the fact that surfactants have a higher affinity for the water–air interface than the benzene–air interface. Unfortunately, accurate data for K and Ma are not available in the literature, even for the most common interfaces and surfactants, for a more precise comparison.

The diffusive-adsorption model is a six-dimensional system with two additional parameters Pe and St. For a given experimental system, Pe and St are dependent on

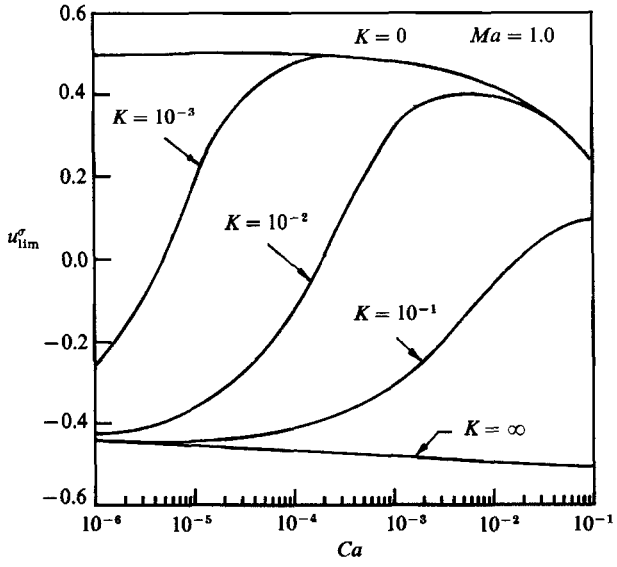

FIGURE 7. The retardation of the limiting cap interfacial velocity from the surfactant-free case of 0.5 (at low Ca) by the Marangoni effect. Even in the limit of infinite adsorption ($K \to \infty$), the bubble does not behave like a rigid one since the interfacial velocity does not approach the bubble speed Ca. The Marangoni number is at $Ma = 1.0$.

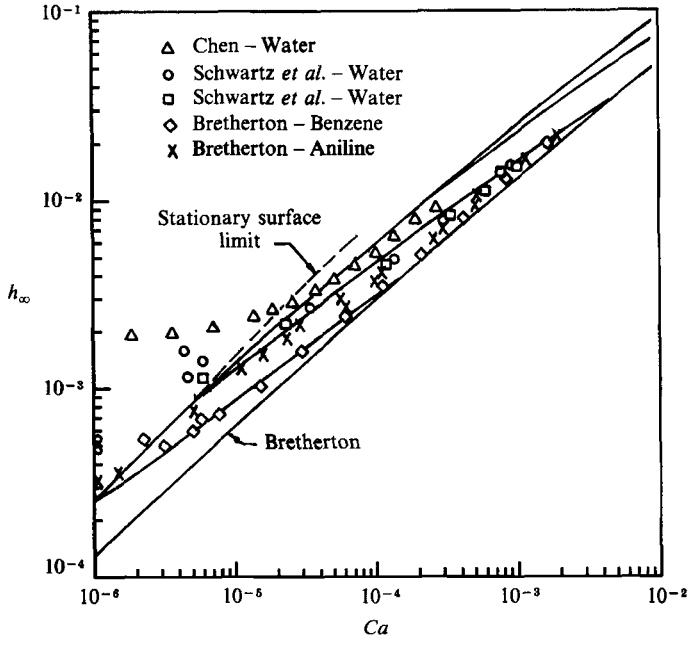

FIGURE 8. Comparison of various film thickness measurements to the computed results from the convective-equilibrium model of figure 4 for $Ma = 1.0$ and $K = 0$, 10^{-3}, 10^{-2}, 10^{-1} and ∞. The maximum limit of the stationary surface model is also shown.

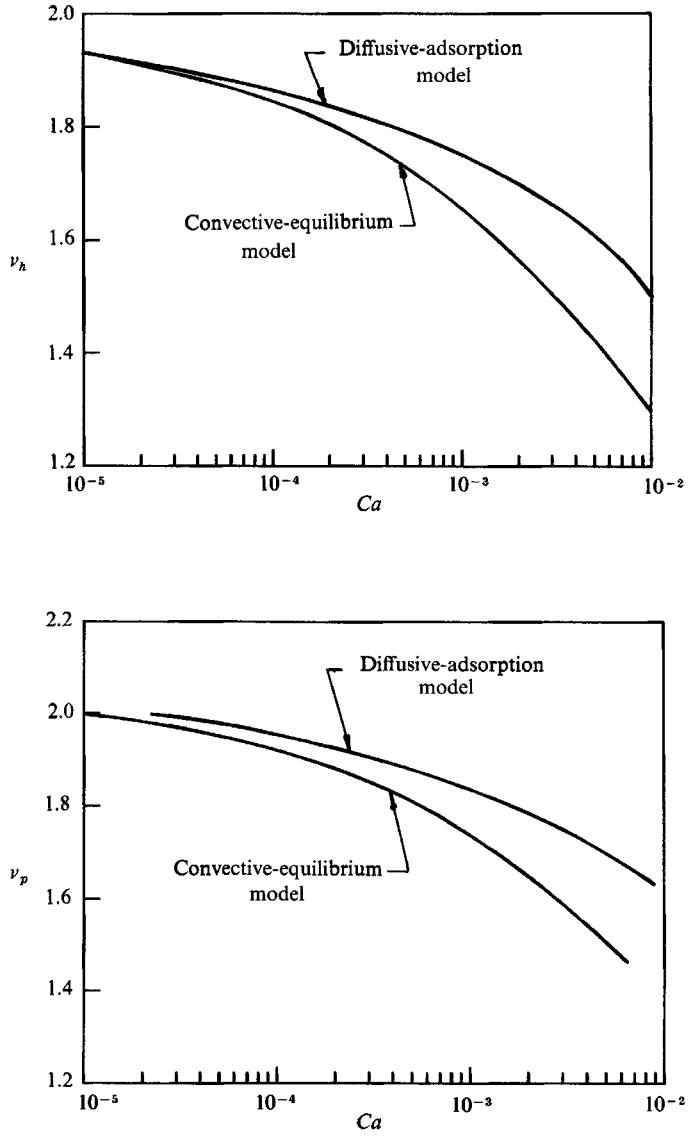

FIGURE 9. The normalized film thickness and cap liquid pressure of the diffusive-adsorption model compared to the convective equilibrium model. The parameters are $Ma = 1.0$, $K = 0.1$, $Pe = 1.0 \times 10^5 Ca$ and $St = 1.0 \times 10^{-6} Ca^{-1}$.

the bubble velocity. To decouple the flow effects, we substituted typical literature values mentioned in §4 to yield

$$Pe = 1.0 \times 10^5 Ca, \quad St = 1.0 \times 10^{-6} Ca^{-1}. \tag{5.8a, b}$$

For this set of Pe and St, we have found that the spectrum of the fixed point

$$(P, \psi, h, u^\sigma, C_0, \Gamma) = \left(\frac{1}{1-h_\infty}, 0, h_\infty, -1, K\Gamma_\infty, \Gamma_\infty\right), \tag{5.9}$$

contains one unstable real eigenvalue, three stable real eigenvalues and a stable complex pair for all Ca, Ma and K values considered. Hence, two additional stable

eigenvectors must be eliminated which constitute the two additional conditions required for the extra degrees of freedom introduced by C_0 and Γ. Consequently, the iteration process remains a one-dimensional problem involving iterating h_∞ to satisfy (5.7). Figure 9 depicts the computed ν_h and ν_p for $Ma = 1.0$ and $K = 1.0$. The film thickness and tip liquid pressure both exceed the convective-equilibrium model. Apparently, bulk gradient caused by axial diffusion more than compensates for surface convection and induces an even larger increase in the film thickness. At low Ca, the stationary surface limit of $4^{\frac{2}{3}}$ in (4.24) is approached from below indicating that $4^{\frac{2}{3}}$ is still the maximum increase for this model.

6. Conclusions and discussions

We have shown that trace amounts of surfactants, $\Gamma \approx O(Ca^{\frac{1}{3}})$, can increase the thickness of a liquid film laid down by a bubble. The mechanism involves a larger surface tension and a lower surfactant concentration in the flat film region than the cap region. For this to occur, bulk diffusion cannot be much faster than bulk convection and adsorption ($Pe > O(1)$) such that a parallel decrease in bulk concentration also occurs into the film region. Surface convection, on the other hand, tends to reduce film thickness. Its negative effect can be neglected if adsorption is faster than surface convection ($St > Ca^{\frac{1}{3}}$). This explains Ginley & Radke's result that the bulk equilibrium model produces a thinner film while the convective-equilibrium model is shown here to yield a thicker film. We have obtained the precise order estimates of Pe and St for the various models. Unfortunately, insufficient data are available for surfactants to ensure that the systems in figure 8 satisfy the derived conditions for a thicker film. Nevertheless, the adsorption rate should slow down as the surface is saturated with a monolayer of surfactants at higher bulk concentrations above the critical micelle concentration. Hence, we expect the assignment $St > Ca^{\frac{1}{3}}$ to be valid only for trace amounts of surfactants/contaminants. This is consistent with our order assignment for Γ in (4.4).

We have only focused on the computation of the film thickness in this study. The pressure drop p in figure 5 corresponds to the pressure drop across the front cap. To compute the pressure drop across the entire bubble, the back half of the bubble must be constructed. However, shooting towards the bubble rear reverses the sign on the eigenvalues in (5.5) and (5.6). Hence, unlike Bretherton's mobile case where only the complex pair (5.5*b*) are unstable, our new models involve yet a third unstable eigenvector corresponding to (5.6). The back half of the bubble may then oscillate as it leaves the flat film as in Bretherton's mobile case or it may feel only the real unstable eigenvalue of (5.6) and increase monotonically. It can also be a linear combination of all three unstable eigenvectors and exhibits both characteristics. In fact, an elaborate numerical iteration scheme must be constructed to choose the appropriate linear combination such that the final trajectory satisfies the symmetry condition at the back tip. It is hence extremely difficult to compute the pressure drop across the entire bubble without resorting to a perturbation analysis for limiting conditions like the one carried out by Ginley & Radke for the bulk equilibrium model. We will be content with the derivation of the film thickness here.

This work was partially supported by NSF contract CBT 8451116, and by ACS-PRF contract 20786-AC7.

REFERENCES

BRETHERTON, F. P. 1961 The motion of long drops and bubbles in tubes. *J. Fluid Mech.* **10**, 166–188.

CHANG, H.-C. & RATULOWSKI, J. 1987 Bubble transport in capillaries. *AIChE Annual Meeting*, November 15–20, New York, paper 681.

CHEN, J. D. 1986 Measuring the film thickness surrounding a bubble inside a capillary. *J. Colloid Interface Sci.* **109**, 34–39.

DAVIS, R. E. & ACRIVOS, A. 1966 The influence of surfactants on the creeping motion of bubbles. *Chem. Engng Sci.* **21**, 681–685.

FAIRBROTHER, F. & STUBBS, A. E. 1935 Studies in electroendosmosis. Part VI. The bubble-tube methods of measurement. *J. Chem. Soc.* **1**, 527–529.

GINLEY, G. M. & RADKE, C. J. 1989 The influence of soluble surfactants on the flow of the long bubbles through a cylindrical capillary. *ACS Symposium Series* 396, pp. 480–501.

GOLDSHTIK, M. A., KHANIN, V. M. & LIGAI, V. G. 1986 A liquid drop on an air cushion as an analogue of Leidenfrost boiling. *J. Fluid Mech.* **166**, 1–20.

GOLDSMITH, H. L. & MASON, S. G. 1963 The flow of suspensions through tubes II. Single large bubbles. *J. Colloid Sci.* **18**, 237–261.

HEDGE, M. G. & SLATTERY, J. C. 1971 Capillary waves at a gas–liquid interface. *J. Colloid Interface Sci.* **35**, 183–199.

HERBOLZHEIMER, E. 1987 The effect of surfactant on the motion of a bubble in a capillary. *AIChE Annual Meeting*, November 15–20, New York, paper 68j.

HIRASAKI, G. J. & LAWSON, J. B. 1985 Mechanisms of foam flow in porous media: Apparent viscosity in smooth capillaries. *Soc. Pet. Engrs J.* **25**, 176–190.

LANDAU, L. & LEVICH, B. 1942 Dragging of a liquid by a moving plate. *Acta Physio-chim. USSR* **17**, 42–45.

LEVICH, B. 1962 *Physiochemical Hydrodynamics*, pp. 415–429. Prentice Hall.

LU, W. Q. & CHANG, H.-C. 1988 An extension of the biharmonic boundary integral method to free surface flow in channels. *J. Comp. Phys.* **77**, 340–360.

MARCHESSAULT, R. N. & MASON, S. G. 1960 *Ind. Chem. Engng* **52**, 79–81.

PARK, C. W. & HOMSY, G. W. 1984 Two-phase displacement in Hele-Shaw cells. *J. Fluid Mech.* **139**, 291–308.

RATULOWSKI, J. 1988 Mathematical modeling of mechanisms in bubble transport: A lubrication approach. PhD thesis, University of Houston.

RATULOWSKI, J. & CHANG, H.-V. 1989 Transport of air bubbles in capillaries. *Phys. Fluids* (in press).

REINELT, D. A. & SAFFMAN, P. G. 1985 The penetration of a finger into a viscous fluid in a channel and a tube. *SIAM J. Sci. Stat. Comput.* **6**, 542–561.

SADHAL, S. S. & JOHNSON, R. E. 1983 Stokes flow past bubbles and drops partially coated with thin films. Part 1. Stagnant cap of surfactant film – exact solution. *J. Fluid Mech.* **126**, 237–250.

SCHWARTZ, L. W., PRINCEN, H. M. & KISS, A. D. 1986 On the motion of bubbles in capillary tubes. *J. Fluid Mech.* **172**, 259–275.

SECOMB, T. W. & SKALAK, R. 1982 Two-dimensional model for capillary flow of an Asymmetric Cell. *Microvascular Res.* **24**, 194–203.

SHEN, E. I. & UDELL, K. S. 1985 A finite element study of low Reynolds number two-phase flow in cylindrical tubes. *J. Appl. Mech.* **107**, 253–256.

TAYLOR, G. I. 1961 Deposition of a viscous fluid on the wall of a tube. *J. Fluid Mech.* **10**, 161–165.

TELETZKE, G. F. 1983 Thin liquid films: Molecular theory and hydrodynamic implications. PhD thesis, University of Minnesota.

WHITAKER, S. & PIERSON, F. W. 1976 Studies of the drop-weight method for surfactant solutions I. Mathematical analysis of the adsorption of surfactants at the surface of a growing drop. *J. Colloid Interface Sci.* **51**, 203–218.

WILSON, S. D. R. 1982 The drag-out problem in film coating theory. *J. Engng Maths* **16**, 209–221.